Korean J. Chem. Eng., **28**(2), 461-469 (2011)
DOI: 10.1007/s11814-010-0371-8

Premixed filtration combustion of micron and sub-micron particles in inert porous media: A theoretical analysis

Mehdi Bidabadi, Jalil Fereidooni, Reza Tavakoli, and Majid Mafi†

Department of Mechanical Engineering, Combustion Research Laboratory,
Iran University of Science and Technology, Narmak, Tehran 16844, Iran
(*Received 17 November 2009 • accepted 30 June 2010*)

Abstract−An analytical model for one-dimensional premixed filtration combustion of volatile fuel particles-air mixture is presented. It is presumed that fuel particles first vaporize and a gaseous fuel with definite chemical structure is formed, which is subsequently oxidized in the gas phase. Flame structure is considered in the three zones. In the preheating vaporization zone, the mixture is heated until it reaches ignition temperature. In the reaction zone, the combustible mixture burns and the post flame zone is occupied by the combustion products. The temperature and mass fraction profiles are obtained of gaseous fuel in these three zones at a semi-infinite inert porous media. Thereafter, the effects of various parameters such as gas velocity, porosity, fuel particles diameter, number density of fuel particles, and heat of chemical reaction on the temperature and mass fraction profiles are investigated.

Key words: Fuel Particles Combustion, Inert Porous Medium, Analytical Solution

INTRODUCTION

In the free laminar premixed flames, flame speed and rate of released heat per unit area depend on conductive heat transfer and thermal radiation of gas mixture. In these flames, temperature is locally high, because there is not adequate heat loss from combustion zone. It also causes pollutions such as NO_x. In the porous media, these limitations have been reduced to an acceptable amount. Filtration combustion includes a heterogeneous exothermic combustion along a porous medium in which a solid, liquid or gas fuel with an oxidizer reacts that pass through this medium [1]. When the gaseous mixture in the porous medium ignites, released heat from this reaction is absorbed by the porous bed and is transmitted to adjacent layers. This process is a type of the process of increasing enthalpy. Gas combustion in porous media is of the most interest, due to its industrial applications, such as oil extraction, infrared burner and heater development, ceramic materials synthesis, porous catalysts, volatile organic compound destruction in the air, diesel engines, and pollution control [2]. In recent decades, porous media burners of gaseous fuel have shown many advantages among the conventional burners. The advantages of porous media burners are high power density, very low emission, very wide power range, combustion stability over wide range of equivalence ratio and high thermal efficiency. These advantages of radiative porous burners have led to their various thermal applications [3].

Filtration combustion includes complex processes, such as chemical kinetics, thermodynamics, combustion theory, and fluid dynamics. A large number of studies on this subject have been performed experimentally [4-7], analytically [8-11], and numerically [1,5,9,12]. Also, a comprehensive review has been done by Howell et al. [2], Kamal and Mohamad [13] and Abdul Mujeebu et al. [14] on this subject.

The feasibility of burning solid fuels in the form of fine powder inside porous media has been numerically investigated by Kayal and Chakravarty [15]. A one-dimensional heat transfer model was developed using the two-flux gray radiation approximation for radiative heat flux equations. The effects of absorption coefficient, emissivity of medium, flame position and reaction enthalpy flux on radiative energy output efficiency have been presented. It was revealed that in porous medium the combustion of suspended carbon particles is similar to premixed single phase gaseous fuel combustion, except that the former has a shorter preheating temperature zone length.

Filtration combustion of carbon is used in various industrial processes, namely, underground coal gasification, in situ combustion for residual oil recovery, and such large-scale production as roasting and sintering of ores, blast-furnace process, and direct reduction of iron from beneficiated iron ores. Becker et al. [16] studied the kinetics of the overall reactions of carbon gasification at temperatures up to 1,600 K. The kinetic characteristics of the reactions are taken into account in a distributed mathematical model of filtration combustion of carbon. By computational experiment at different values of process control parameters (the gas flow rate, the fraction of the oxidant in the gas, and the mass ratio of carbon to the inert material in the combustible mixture), it was found that, in the wave of filtration combustion of carbon under superadiabatic conditions, carbon gasification can predominately yield either CO_2 or CO.

Bubnovich et al. [10] performed an analytical study of combustion waves during the filtration of lean methane-air mixtures in inert porous media using the one-temperature approximation. The analytical solution was built in three different regions: the preheating region, the reaction region and the region occupied by the combustion products. Analytic expressions predicting the temperature and methane mass fraction profiles in the wave, as well as, the combustion wave velocity and the longitudinal extension of the reac-

†To whom correspondence should be addressed.
E-mail: Majid.Mafi@gmail.com

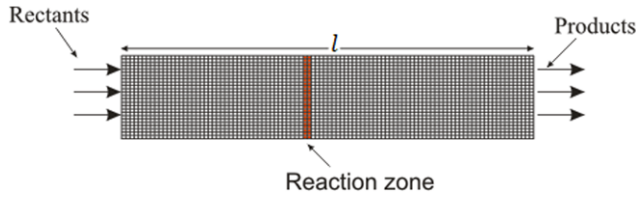

Fig. 1. Schematic diagram of combustion system in a porous medium.

tion region were derived.

This study was aimed at investigating the filtration combustion of uniformly distributed volatile fuel particles in air. For this, an analytical model based on analytical solution presented by Bubnovich et al. [10] is developed. The temperature profile obtained is compared with that of the analytical study of Bubnovich et al. [10]. The effects of varying parameters such as gas velocity, and porosity on the temperature and mass fraction profiles of gaseous fuel in all pre-combustion, combustion and post-combustion flame zones are also analyzed.

MATHEMATICAL MODEL

Fig. 1 shows a schematic illustration of the porous media combustor. Combustible mixture enters to the inert porous medium combustor with a length of l at ambient temperature with uniform velocity. In the initial part of the channel the mixture inflames and a narrow reaction zone is formed with a thickness of l_{II} moving in the direction of fuel flow with uniform velocity u_{FC}. The entire region of combustion is divided into three regions. The preheat zone begins from entrance edge of flow into the channel to the location that mixture temperature reaches the ignition temperature. The chemical reaction region is defined from the end of the first zone to where reaction is completed and finished. The last region is the post-combustion region, which is occupied by the combustion products.

The chemical reaction of combustion process is modeled as a one-step overall reaction

$$\nu_F[\mathrm{F}]+\nu_{O_2}[\mathrm{O_2}]+\text{inert component}\rightarrow \nu_p[\mathrm{P}]+\text{inert component} \tag{1}$$

where the symbols F, O_2, and P denote the fuel, oxygen and product, respectively, and the quantities ν_F, ν_{O_2} and ν_p denote their respective stoichiometric coefficients.

Modeling of filtration combustion of combustible mixture including uniformly distributed volatile fuel particles in air involves conservation equations for species and energy and boundary conditions prescribed on problem. Here a one-dimensional model of the problem is presented and solved. All external forces including gravitational effects are assumed to be negligible. Other introduced approximations are that diffusion caused by pressure gradient is negligible and Soret and Dufour effects are negligibly small. For simplicity it is assumed that solid temperature and gaseous fuel temperature are approximately equal to the oxidizing gas temperature.

$$\frac{\partial \mathrm{Y}}{\partial \mathrm{t}}+\mathrm{u}_g\frac{\partial \mathrm{Y}}{\partial \mathrm{z}}=\frac{\partial}{\partial \mathrm{z}}\left(\mathrm{D}\frac{\partial \mathrm{Y}}{\partial \mathrm{z}}\right)+\frac{\mathrm{w}_v}{\rho_g}-\frac{\mathrm{w}_F}{\rho_g} \tag{2}$$

$$[\varepsilon(\rho \mathrm{c}_p)_g+(1-\varepsilon)(\rho \mathrm{c}_p)_s]\frac{\partial \mathrm{T}}{\partial \mathrm{t}}+\varepsilon(\rho \mathrm{c}_p)_g\mathrm{u}_g\frac{\partial \mathrm{T}}{\partial \mathrm{z}}$$

$$=\frac{\partial}{\partial \mathrm{z}}\left(\lambda\frac{\partial \mathrm{T}}{\partial \mathrm{z}}\right)-\mathrm{h}_{eff}(\mathrm{T}-\mathrm{T}_0)-\varepsilon \mathrm{Q}_v\mathrm{w}_v+\varepsilon \mathrm{Q}\mathrm{w}_F, \tag{3}$$

where Q is the heat release per unit mass of consumed gaseous fuel, Q_v is the heat associated with vaporizing per unit mass of fuel and h_{eff} is the heat transfer coefficient to surroundings per unit of tube diameter d_t.

Thermal conductivity of the porous media λ can be written in the form

$$\lambda=\varepsilon\lambda_g+(1-\varepsilon)\lambda_s+\lambda_{rad} \tag{4}$$

Radiation is a significant heat transfer mechanism in the solid phase of packed bed; it enhances the heat transfer in the bed and broadens the reaction zone. The extended reaction zone exhibits intense superficial radiation from the packed material, but due to multiple reflections it is essentially contained within an approximate length equal to the tube diameter. Thus, the gas in this region can be treated as a thick gas for computation [17]. For simplicity a radiation term is added to the gas and solid thermal conductivity by a radiant conductivity model [18]

$$\lambda_{rad}=\frac{32\varepsilon\sigma \mathrm{d}_s\mathrm{T}_s^3}{9(1-\varepsilon)}, \tag{5}$$

where σ is the Stephan-Boltzmann constant.

In the analysis it is assumed that the fuel particles vaporize first to yield a gaseous fuel of known chemical structure, which is subsequently oxidized in the gas phase. Thus, surface reactions are neglected. The kinetics of vaporization are assumed to be represented by the expression [19]

$$\mathrm{w}_v=\mathrm{An}_s\pi \mathrm{d}_p^2\mathrm{T}_g^n, \tag{6}$$

where the quantities A and n are constants which are assumed to be known, n_s is the local number density of particles and T denotes the gas temperature.

Reaction rate of species can be written in the form [20]

$$\mathrm{w}_F=\rho_g \mathrm{k}_0\mathrm{Y}_F\mathrm{e}^{-E/RT}, \tag{7}$$

where k_0, E and R are the pre-exponential factor, activation energy and universal gas constant, respectively.

Here, a coordinate system x attaching to the reaction region is defined

$$\mathrm{x}=\mathrm{z}-\mathrm{z}(\mathrm{t}), \tag{8}$$

where z(t) is the location of the reaction zone and therefore $u_{FC}=\dot{z}(t)$ is reaction front velocity. Mathematical model after using this new moving coordinate with assuming n=1 in dimensionless form is

$$\frac{\partial \overline{\mathrm{Y}}}{\partial \overline{\mathrm{x}}}=\xi\frac{\partial^2\overline{\mathrm{Y}}}{\partial \overline{\mathrm{x}}^2}+\eta\overline{\mathrm{T}}+\zeta-\mu\overline{\mathrm{Y}}\mathrm{e}^{-E/RT} \tag{9}$$

$$\alpha\frac{\partial \overline{\mathrm{T}}}{\partial \overline{\mathrm{x}}}=\frac{\partial^2\overline{\mathrm{T}}}{\partial \overline{\mathrm{x}}^2}-\beta\overline{\mathrm{T}}-\nu+\gamma\overline{\mathrm{Y}}\mathrm{e}^{-E/RT}, \tag{10}$$

where dimensionless parameters are

$$\overline{\mathrm{x}}=\frac{\mathrm{x}}{\mathrm{X}},\quad \overline{\mathrm{Y}}=\frac{\mathrm{Y}}{\mathrm{Y}_0},\quad \mathrm{X}=\frac{\lambda}{(\rho \mathrm{c}_p)_g(\mathrm{u}_g-\mathrm{u}_{FC})},$$

$$\mathrm{Y}_0=\frac{(\varepsilon \mathrm{c}_{p,g}+(1-\varepsilon)\mathrm{c}_{p,s})(\mathrm{T}_{ig}-\mathrm{T}_0)}{\mathrm{Q}}$$

$$\bar{l}=\frac{l_I}{X},\ \delta=\frac{l_{II}}{X},\ \overline{T}=\frac{T-T_0}{T_{ig}-T_0},\ Le=\frac{\lambda_g}{(\rho c_p)_g D},\ \overline{\lambda}=\frac{\lambda_g}{\lambda},\ \xi=\frac{\overline{\lambda}}{Le}$$

$$\eta=\frac{An_s\pi d_p^2\lambda(T_{ig}-T_0)}{Y_0\rho_g^2 c_{p,g}(u_g-u_{FC})^2},\ \zeta=\frac{\eta T_0}{(T_{ig}-T_0)},\ \mu=\frac{k_0\lambda}{(\rho c_p)_g(u_g-u_{FC})^2}$$

$$\alpha=\varepsilon-\frac{(1-\varepsilon)(\rho c_p)_s u_{FC}}{(\rho c_p)_g(u_g-u_{FC})},\ \beta=\frac{h_{eff}\lambda}{[(\rho c_p)_g(u_g-u_{FC})]^2}+\frac{\varepsilon An_s\pi d_p^2 Q_1\lambda}{[(\rho c_p)_g(u_g-u_{FC})]^2}$$

$$\nu=\frac{\varepsilon An_s\pi d_p^2 Q_1\lambda T_0}{(T_{ig}-T_0)[(\rho c_p)_g(u_g-u_{FC})]^2},\ \gamma=\frac{\varepsilon Q k_0 Y_0\lambda}{\rho_g c_{p,g}^2(u_g-u_{FC})^2(T_{ig}-T_0)},$$

where $\overline{Y}$ is the so called dimensionless mass fraction. The structure of the flame is assumed to consist of three regions: a preheat vaporization zone, a reaction zone and the region occupied by the combustion products. Boundary conditions with these descriptions are as follows:

$$\text{at } \bar{x}=-\bar{l}:\ \overline{T}_1=0,\ \overline{Y}_1=0 \tag{12}$$

$$\text{at } \bar{x}=0:\ \overline{T}_1=\overline{T}_2=1,\ \left(\frac{\partial\overline{T}}{\partial\bar{x}}\right)_1=\left(\frac{\partial\overline{T}}{\partial\bar{x}}\right)_2,\ \overline{Y}_1=\overline{Y}_2 \tag{13}$$

$$\text{at } \bar{x}=\delta:\ \overline{T}_2=\overline{T}_3,\ \left(\frac{\partial\overline{T}}{\partial\bar{x}}\right)_2=\left(\frac{\partial\overline{T}}{\partial\bar{x}}\right)_3,\ \overline{Y}=\Lambda \tag{14}$$

$$\text{at } \bar{x}=+\infty:\ \overline{T}=0,\ \overline{Y}=0 \tag{15}$$

ANALYTICAL SOLUTION

Fig. 2 shows a schematic illustration of the presumed flame structure in porous medium. It consists of a broad preheat-vaporization zone, a thin reaction zone, and a broad post-flame zone. To solve the conservation equations governing in this environment and to determine the structure of these regions, a series of assumptions is considered which will be brought in each region separately.

1. Preheat-vaporization Zone

For simplicity, it is assumed that in all regions the properties of mixtures are constant and Lewis number Le is unity. In the preheat-vaporization zone the rate of chemical reaction between the fuel and oxidizer is assumed to be small, and the structure of this layer is determined from a balance between the convective, diffusive, and vaporization terms in the conservation equations. First, the energy equation and then the species conservation equation will be solved. The temperature distribution in this area is as follows:

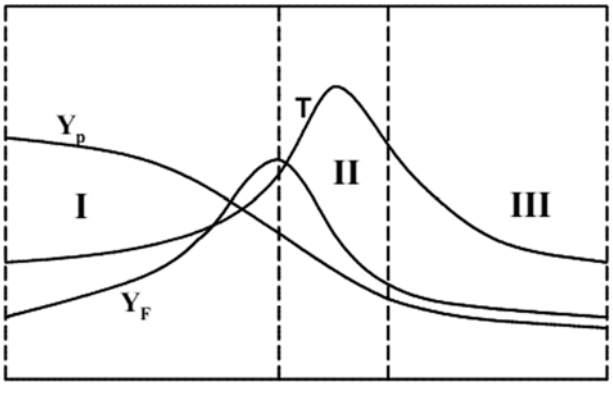

Fig. 2. Schematic illustration of the presumed structure of the flame.

$$\overline{T}_1=c_1e^{r_1\bar{x}}+c_2e^{r_2\bar{x}}-\frac{\nu}{\beta} \tag{16}$$

$$r_1=\frac{\alpha-\sqrt{\alpha^2+4\beta}}{2},\ r_2=\frac{\alpha+\sqrt{\alpha^2+4\beta}}{2} \tag{17}$$

With boundary conditions $\overline{T}_1=0$ at $\bar{x}=-\bar{l}$ and $\overline{T}_1=1$ at $\bar{x}=0$ constants c_1 and c_2 are found.

$$c_1=\frac{\nu/\beta-(1+\nu/\beta)e^{-r_2\bar{l}}}{e^{-r_1\bar{l}}-e^{-r_2\bar{l}}},\ c_2=\frac{(1+\nu/\beta)e^{-r_1\bar{l}}-\nu/\beta}{e^{-r_1\bar{l}}-e^{-r_2\bar{l}}} \tag{18}$$

With the temperature distribution, (9) can be resolved and distribution of the mass fraction of the gaseous fuel is obtained. For this purpose, it is assumed that the temperature appeared in the exponential term of (9) is constant and equal to the mean value of the initial temperature of the mixture and the ignition temperature. As a result, there is

$$\mu_I=\mu e^{-2E/R(T_0+T_{ig})} \tag{19}$$

$$\overline{Y}_I=d_1e^{k_1\bar{x}}+d_2e^{k_2\bar{x}}-\frac{\eta c_1}{\xi r_1^2-r_1-\mu_I}e^{r_1\bar{x}}-\frac{\eta c_2}{\xi r_2^2-r_2-\mu_I}e^{r_2\bar{x}}+\frac{\zeta-\eta\nu/\beta}{\mu_I} \tag{20}$$

$$k_1=\frac{1-\sqrt{1+4\xi\mu_I}}{2\xi},\ k_2=\frac{1+\sqrt{1+4\xi\mu_I}}{2\xi} \tag{21}$$

2. Chemical Reaction Region

In the second zone the vaporization terms are assumed to be small in comparison with the convective, diffusive and reactive terms. In this thin region is also assumed that in the exponential terms the temperature is constant and equal to the ignition temperature. With these assumptions,

$$\mu_{II}=\mu e^{-E/(RT_{ig})} \tag{22}$$

$$\overline{Y}_{II}=d_3e^{k_3\bar{x}}+d_4e^{k_4\bar{x}} \tag{23}$$

$$k_3=\frac{1-\sqrt{1+4\xi\mu_{II}}}{2\xi},\ k_4=\frac{1+\sqrt{1+4\xi\mu_{II}}}{2\xi} \tag{24}$$

Here, for the general solution (23), because k_4 is positive, the second term is cancelled and $d_4=0$. By using the boundary conditions $\overline{Y}_1=0$ at $\bar{x}=-\bar{l}$ and $\overline{Y}_1=\overline{Y}_2$ and $\overline{\dot{Y}}_1=\overline{\dot{Y}}_2$ at $\bar{x}=0$ the values of d_1, d_2 and d_3 are obtained in a system of linear equations. The solution of the system by Cramer's rule [21] is given by

$$d_1=\frac{\begin{vmatrix} A & e^{-k_2\bar{l}} & 0 \\ B & 1 & -1 \\ C & k_2 & -k_3 \end{vmatrix}}{\begin{vmatrix} e^{-k_1\bar{l}} & e^{-k_2\bar{l}} & 0 \\ 1 & 1 & -1 \\ k_1 & k_2 & -k_3 \end{vmatrix}} \tag{25}$$

$$d_2=\frac{\begin{vmatrix} e^{-k_1\bar{l}} & A & 0 \\ 1 & B & -1 \\ k_1 & C & -k_3 \end{vmatrix}}{\begin{vmatrix} e^{-k_1\bar{l}} & e^{-k_2\bar{l}} & 0 \\ 1 & 1 & -1 \\ k_1 & k_2 & -k_3 \end{vmatrix}} \tag{26}$$

$$d_3=\frac{\begin{vmatrix} e^{-k_1\bar{l}} & e^{-k_2\bar{l}} & A \\ 1 & 1 & B \\ k_1 & k_2 & C \end{vmatrix}}{\begin{vmatrix} e^{-k_1\bar{l}} & e^{-k_2\bar{l}} & 0 \\ 1 & 1 & -1 \\ k_1 & k_2 & -k_3 \end{vmatrix}} \tag{27}$$

where constants A, B and C are as follows:

$$A=\frac{\eta c_1}{\xi r_1^2-r_1-\mu_I}e^{-r_1\bar{l}}+\frac{\eta c_2}{\xi r_2^2-r_2-\mu_I}e^{-r_2\bar{l}}-\frac{\zeta-\eta\nu/\beta}{\mu_I} \tag{28}$$

$$B=\frac{\eta c_1}{\xi r_1^2-r_1-\mu_I}+\frac{\eta c_2}{\xi r_2^2-r_2-\mu_I}-\frac{\zeta-\eta\nu/\beta}{\mu_I} \tag{29}$$

$$C=\frac{\eta c_1 r_1}{\xi r_1^2-r_1-\mu_I}+\frac{\eta c_2 r_2}{\xi r_2^2-r_2-\mu_I} \tag{30}$$

With a gaseous fuel mass fraction profile, the temperature profile will be obtained.

$$\beta_{II}=\frac{h_{eff}\lambda_{eff}}{[(\rho c_p)_g(u_g-u_{FC})]^2} \tag{31}$$

$$\gamma_{II}=\gamma e^{-E/(RT_{ig})} \tag{32}$$

$$\overline{T}_{II}=c_3e^{r_3\bar{x}}+c_4e^{r_4\bar{x}}-\frac{\gamma_{II}d_3}{k_3^2-\alpha k_3-\beta_{II}}e^{k_3\bar{x}} \tag{33}$$

$$r_3=\frac{\alpha-\sqrt{\alpha^2+4\beta_{II}}}{2},\quad r_4=\frac{\alpha+\sqrt{\alpha^2+4\beta_{II}}}{2} \tag{34}$$

3. Post-combustion Region

In the case of rather slow addition of the oxidizer or a high temperature, the reagents are consumed completely. Considering the small amount of Λ in this region, $\overline{Y}$ is close to zero. However, for the mass fraction profile in the third area, Eq. (23) is used. To acquire the temperature profiles, it is assumed that vaporization and reactive terms are small in comparison with other terms.

$$\overline{Y}_{III}=d_3e^{k_3\bar{x}} \tag{35}$$

$$\overline{T}_{III}=c_5e^{r_3\bar{x}}+c_6e^{r_4\bar{x}} \tag{36}$$

With the boundary condition $\overline{T}=0$ at $\bar{x}=+\infty$, $c_6=0$ is obtained. With boundary conditions $\overline{T}_I=\overline{T}_{II}$ at $\bar{x}=0$, $\overline{T}_{II}=\overline{T}_{III}$ at $\bar{x}=\delta$ and $\dot{\overline{T}}_{II}=\dot{\overline{T}}_{III}$ at $\bar{x}=\delta$ the values of c_3, c_4 and c_5 are obtained in a system of linear equations by Cramer's rule.

$$c_3=\frac{\begin{vmatrix} D & 1 & 0 \\ E & e^{r_4\delta} & -e^{r_3\delta} \\ F & r_4e^{r_4\delta} & -r_3e^{r_3\delta} \end{vmatrix}}{\begin{vmatrix} 1 & 1 & 0 \\ e^{r_3\delta} & e^{r_4\delta} & -e^{r_3\delta} \\ r_3e^{r_3\delta} & r_4e^{r_4\delta} & -r_3e^{r_3\delta} \end{vmatrix}} \tag{37}$$

$$c_4=\frac{\begin{vmatrix} 1 & D & 0 \\ e^{r_3\delta} & E & -e^{r_3\delta} \\ r_3e^{r_3\delta} & F & -r_3e^{r_3\delta} \end{vmatrix}}{\begin{vmatrix} 1 & 1 & 0 \\ e^{r_3\delta} & e^{r_4\delta} & -e^{r_3\delta} \\ r_3e^{r_3\delta} & r_4e^{r_4\delta} & -r_3e^{r_3\delta} \end{vmatrix}} \tag{38}$$

$$c_5=\frac{\begin{vmatrix} 1 & 1 & D \\ e^{r_3\delta} & e^{r_4\delta} & E \\ r_3e^{r_3\delta} & r_4e^{r_4\delta} & F \end{vmatrix}}{\begin{vmatrix} 1 & 1 & 0 \\ e^{r_3\delta} & e^{r_4\delta} & -e^{r_3\delta} \\ r_3e^{r_3\delta} & r_4e^{r_4\delta} & -r_3e^{r_3\delta} \end{vmatrix}} \tag{39}$$

where constants D, E and F are as follows:

$$D=1+\frac{\gamma_{II}d_3}{k_3^2-\alpha k_3-\beta_{II}} \tag{40}$$

$$E=\frac{\gamma_{II}d_3}{k_3^2-\alpha k_3-\beta_{II}}e^{k_3\delta} \tag{41}$$

$$F=Ek_3 \tag{42}$$

4. Reaction Region Thickness and Combustion Wave Velocity

The dimensionless reaction region thickness is unknown in the obtained relations. Regarding the combustion region, it can be said that it starts where the temperature is equal to the ignition temperature, $\overline{T}=1$, and ends in $\bar{x}=\delta$ where the mass fraction of combustible is close to zero ($\overline{Y}=\Lambda$). From (23)

$$\Lambda=d_3e^{k_3\delta}\Rightarrow\delta=\frac{1}{k_3}\ln\frac{\Lambda}{d_3} \tag{43}$$

Therefore, the reaction region thickness can be calculated by means of a value of Λ. Here, the mass fraction of gaseous fuel is assumed to be 1/100 of the value of Y_0.

Combustion wave propagation velocity can be obtained from boundary condition $\dot{\overline{T}}_I=\dot{\overline{T}}_{II}$ at $\bar{x}=0$ which an implicit relation is obtained.

$$\frac{\nu/\beta-(1+\nu/\beta)e^{-r_2\bar{l}}}{e^{-r_1\bar{l}}-e^{-r_2\bar{l}}}\frac{\alpha-\sqrt{\alpha^2+4\beta}}{2}+\frac{(1+\nu/\beta)e^{-r_1\bar{l}}-\nu/\beta}{e^{-r_1\bar{l}}-e^{-r_2\bar{l}}}\frac{\alpha+\sqrt{\alpha^2+4\beta}}{2}$$
$$-c_3\frac{\alpha-\sqrt{\alpha^2+4\beta_{II}}}{2}-c_4\frac{\alpha+\sqrt{\alpha^2+4\beta_{II}}}{2}+\frac{\gamma_{II}d_3}{k_3^2-\alpha k_3-\beta_{II}}k_3=0, \tag{44}$$

where c_3, c_4 and d_3 are obtained from (37), (38) and (27), respectively.

RESULTS AND DISCUSSION

In this paper, filtration combustion of uniformly distributed fuel particles in an oxidizing gas is modeled. For analyzing the results, it is assumed that the gaseous fuel that evolves from the fuel particles is methane [19] and physical properties $c_{p,g}=947e^{0.000183T_g}$ J/(kg K), $\rho_g=1.13$ kg/m^3 and $\lambda_g=4.82\times10^{-7}c_{p,g}T_g^{0.7}$ W/(mK) for the mixture are considered. Combustion of the mixture is described as a single-step overall chemical reaction that released heat per unit mass of consumed fuel is equal to Q=50150000 J/kg and Q_v is equal to 0.01Q. The reaction rate obeys first-order Arrhenius relation with the activation energy E=129999.97 J/mol and pre-exponential factor $k_0=2.6\times10^8$ s^{-1}. For the vaporization term, values of $A=3.713\times10^{-4}$ kg/(m^2 Ks) and n=1 is chosen to be equal to rate of devolatilization of coal at T=1400 K [22]. The value of n_s is 4×10^9 m^{-3} except in those charts in which the effects of its variation are considered.

It is assumed that the semi-infinite porous channel is made up of

5.6 mm diameter alumina spheres forming porosity of ε=0.4 between particles [11]. These alumina spheres have a density ρ_s=3987 kg/m^3, specific heat capacity $c_{p,s}$=29.567+2.61177T_s–0.00171T_s^2+3.382×10^{-7} T_s^3 J/(kg K) and thermal conductivity λ_s=–0.21844539+0.00174653T_s +8.2266×10^{-8}T_s^2 W/(mK). Heat transfer coefficient to surroundings per unit of tube diameter d_t is

$$h_{eff}=\frac{4}{d_t}\left(h+\varepsilon'\varepsilon''\sigma\frac{T^4-T_0^4}{T-T_0}\right), \quad (45)$$

where ε'=0.45 is the emissivity of the solid spheres, ε''=0.38 is the transmissivity factor for the pipe materials, h=10 W/(m^2 K) is the heat transfer coefficient and is the Stefan-Boltzmann constant.

For simplicity, properties of the mixture are regarded as constant. Values of l_f=0.25 m, T_0=300 K, Tig=1150 K, $c_{p,g}$=1087.8 J/(kg K), λ_g=0.0531 W/(m K), λ_s=1.1445 W/(m K) and λ=1.1652 W/(m K) are chosen and value of h_{eff} is considered to be 1,000 W/(m^3 K), except for those charts in which the effect of heat loss from lateral surfaces has been assessed. Therefore, by considering u_g=0.8 m/s and for particles with the diameter of 3 μm, combustion wave displacement speed from (44) is obtained approximately u_{FC}=1.3×10^{-4} m/s.

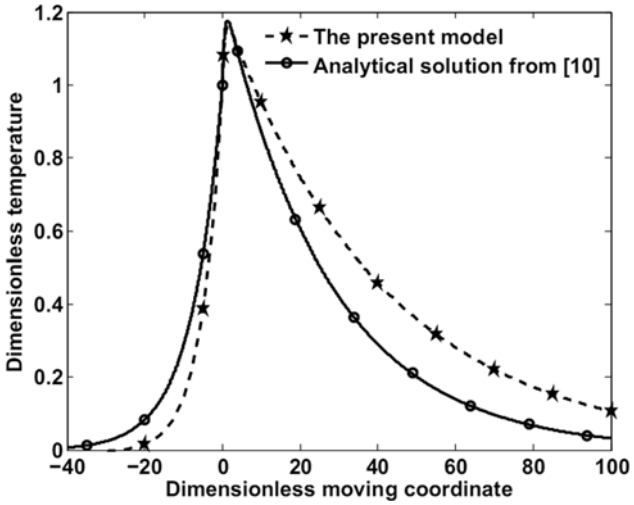

Fig. 3. Comparison between the predictions of the present analytical model for particles of diameter 5 μm and analytical solution by Bubnovich et al. [10] for methane-air mixture under similar conditions.

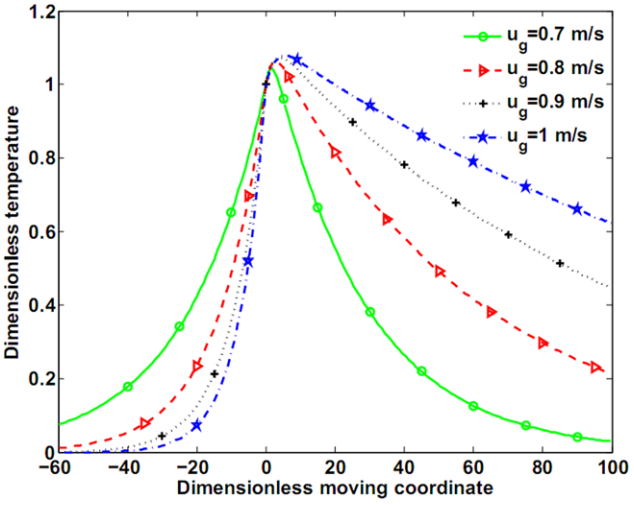

Fig. 4. Dimensionless temperature $\overline{T}$ versus dimensionless moving coordinate in different gas velocity for particles with the diameter of d=3 μm.

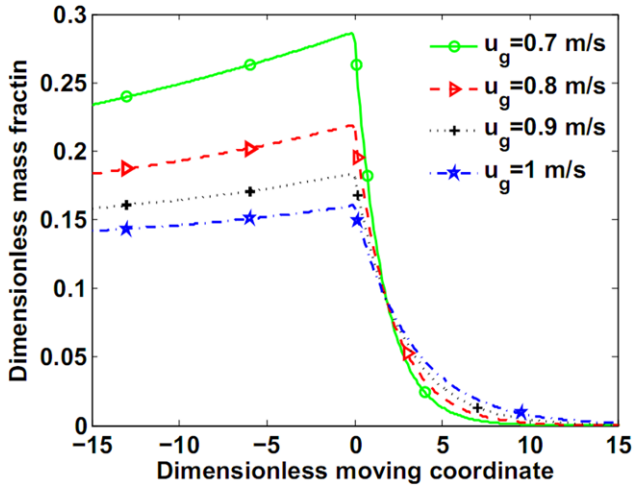

Fig. 5. Dimensionless gaseous fuel mass fraction versus dimensionless moving coordinate in different gas velocity for particles with the diameter of d=3 μm.

Since there are no analytical, experimental or numerical studies similar to this study, the obtained results for particles with 5 micron diameter are compared with the analytical solution of premixed combustion of methane-air mixture at identical conditions performed by Bubnovich et al. [10]. Fig. 3 shows that in the first and the second zones of the flame, the temperature of the particle-air mixture is lower than that of the methane-air mixture, and in the last zone vice versa. Therefore, the predicted maximum temperature for the particle-air mixture is lesser.

Figs. 4 and 5 show variation of dimensionless temperature $\overline{T}$ and dimensionless mass fraction of the gaseous fuel $\overline{Y}$ defined in (11) versus dimensionless moving coordinate in different gas velocities with the assumption of constant combustion wave velocity u_{FC}=1.3×10^{-4} m/s for the particles with the diameter of d=3 μm. By increasing the gas velocity from 0.7 m/s to 1 m/s, the process of the temperature increase is delayed, but by initiating, the slope of increasing of the gas temperature increases and reaches to higher maximum temperature in the combustion zone. The slope of decreasing of the temperature decreases during and after combustion, and in the farther distance from combustion zone, the gas temperature reaches to ambient temperature. In Fig. 4 according to the definition of Y_0 in (11) that does not depend on gas velocity, by increasing of gas velocity, at first, the mass fraction of gaseous fuel Y has a lower value, but because slope of decreasing of the mass fraction decreases during and after combustion, in the larger distance from the first zone approaches to zero.

In Figs. 6 and 7 dimensionless temperature $\overline{T}$ and dimensionless gaseous fuel mass fraction $\overline{Y}$ charts as a function of dimensionless moving coordinate $\overline{x}$ is depicted in various porosities with assumption of constant combustion wave velocity for particles with diameter d=3 μm. The effect of porosity increase on the temperature

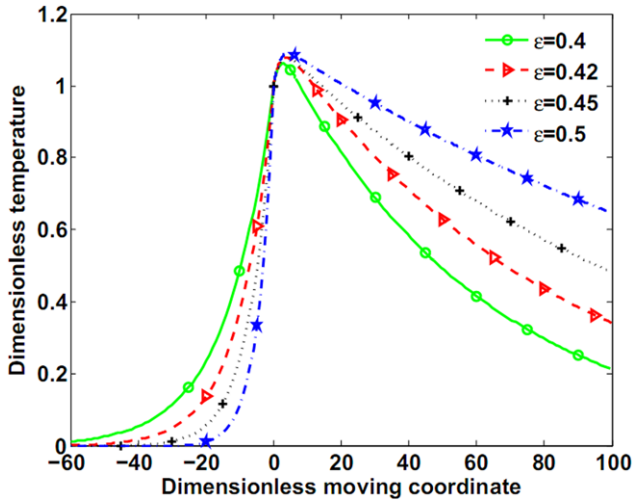

Fig. 6. Dimensionless temperature $\overline{T}$ versus dimensionless moving coordinate in different porosity for particles with the diameter of d=3 μm.

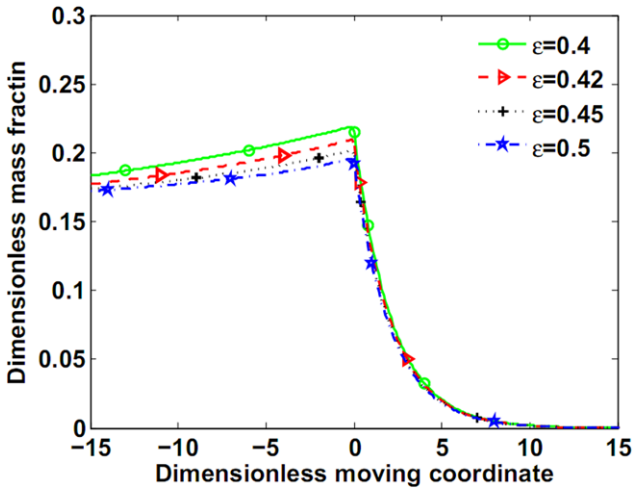

Fig. 7. Dimensionless gaseous fuel mass fraction versus dimensionless moving coordinate in different porosity for particles with the diameter of d=3 μm.

distribution resembles the effect of increasing of gas velocity. It means that by increasing of porosity from 0.4 to 0.5 in the first zone, the temperature decreases, and afterwards temperature increases. Due to the weak dependence of Y_0 on porosity, the increase of porosity causes that the mass fraction of gaseous fuel Y at the end of first zone has a lower value, but at the beginning and middle of the first zone and second and third zones, the increase of porosity from 0.4 to 0.5 has no considerable influence on the mass fraction profile of the gaseous fuel.

Figs. 8-11 show the effect of particle diameter and the number density n_s on the dimensionless temperature profile and dimensionless mass fraction, with the assumption of constant combustion wave velocity. Because in Figs. 8 and 9, in contrast to other charts, the nano-sized diameter is also used; it is assumed that Λ=0.0001. Particle diameter increase or number density of particles has no effect on temperature distribution in the preheat zone. In the combustion

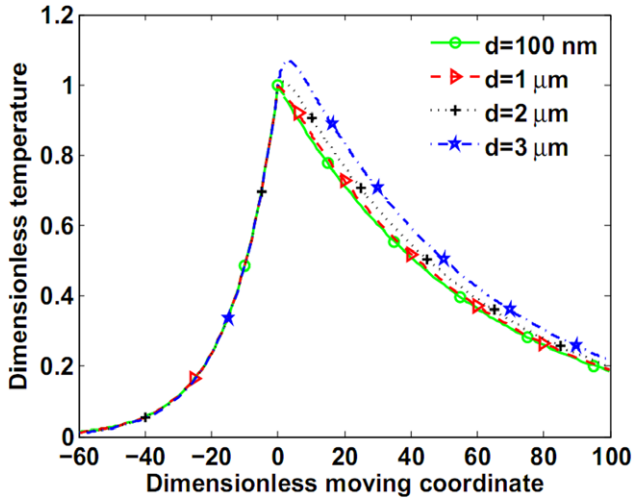

Fig. 8. The effect of the particles diameter increase on the dimensionless temperature profile.

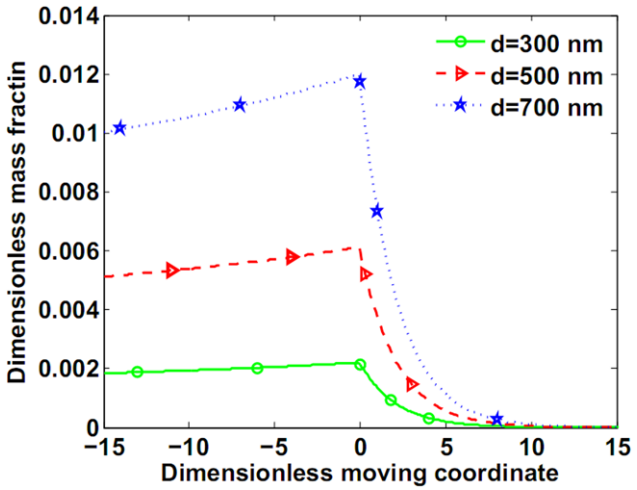

Fig. 9. The effect of the particles diameter increase on the dimensionless mass fraction profile.

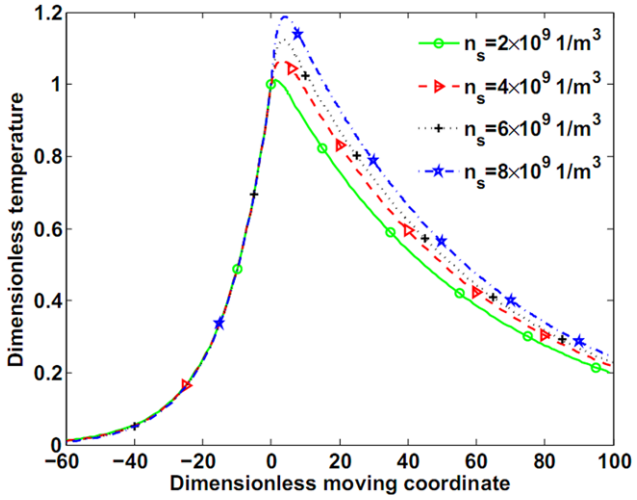

Fig. 10. The effect of the number density variations on the dimensionless temperature profile for particles with the diameter of d=3 μm.

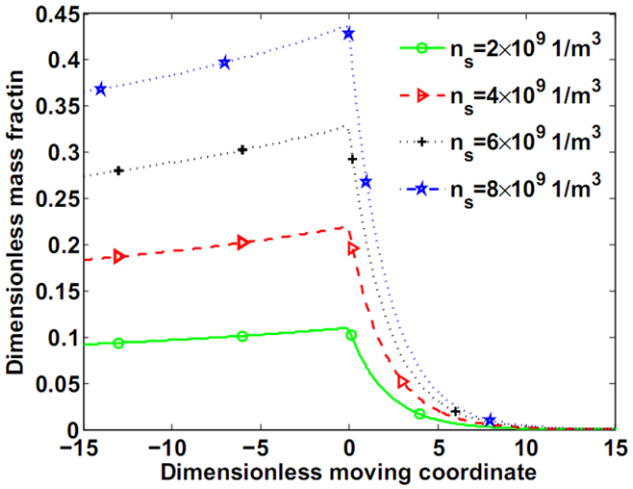

Fig. 11. The effect of the number density variations on the dimensionless mass fraction profile for particles with the diameter of d=3 μm.

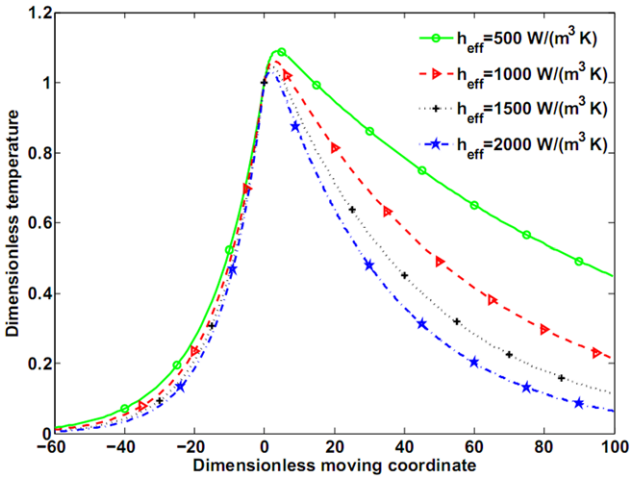

Fig. 12. The effect of increasing of the heat loss of the system from lateral surfaces on temperature distribution for particles with the diameter of d=3 μm.

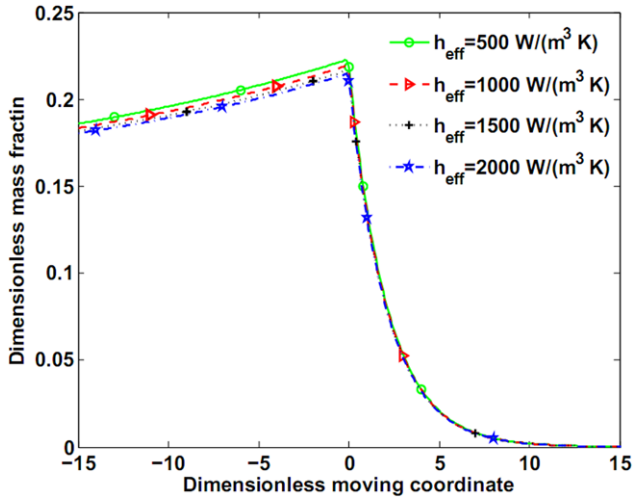

Fig. 13. The effect of increasing of the heat loss from lateral surfaces on the mass fraction distribution for particles with the diameter of d=3 μm.

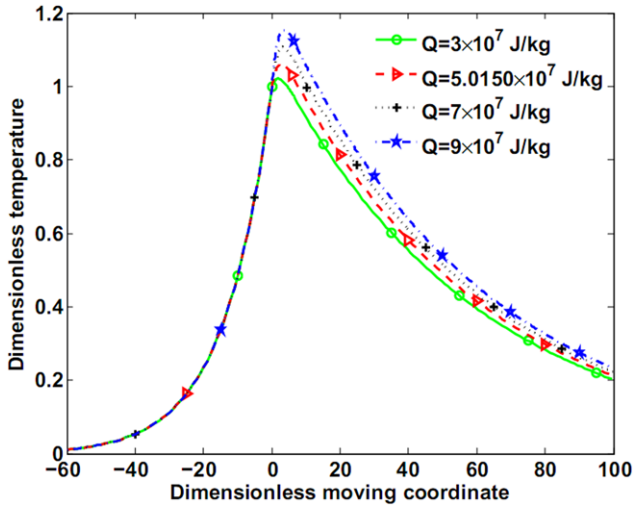

Fig. 14. The effect of the combustion enthalpy variations on the dimensionless temperature profile for particles with the diameter of d=3 μm.

and post-flame zones, these increases are equivalent to the temperature increase. The mass fraction of gaseous fuel Y has also higher values in all zones by particle diameter or number density increases, owing to the increase of vaporization rate of fuel particles.

The effect of the heat loss from lateral surfaces of the system by natural convection and thermal radiation on the temperature distribution and mass fraction is shown in Figs. 12 and 13. As expected, by increasing of the heat loss from the system, the gas temperature decreases. The mass fraction of gaseous fuel also decreases due to the temperature and therefore vaporization rate of fuel particles decrease, but this is negligibly small in the second and third zones.

Fig. 14 is related to the effect of the combustion enthalpy, with the assumption of constant combustion wave velocity and Q_v. As seen, because the chemical reaction is ignored in the preheating zone, there is no variation in the temperature distribution in this zone. The temperature profile is proportional to the heat of reaction in the combustion and post-combustion zones.

CONCLUSIONS

Theoretical analysis of filtration combustion of a combustible mixture, including volatile fuel particles which are propagated uniformly in an oxidizer, is presented. The temperature and mass fraction profiles of the gaseous fuel are obtained analytically in a semi-infinite inert porous media. The analytical results show that for particles with 5 micron diameters at identical conditions, the anticipated maximum temperature for the particles-air mixture is lower than that of the methane-air mixture. Analytical results also indicate that by the gas velocity and porosity increases, that temperature decreases first in the preheat zone and then increases in the combustion and post-combustion zones. By increasing of the gas velocity, at first the mass fraction of gaseous fuel Y decreases, but since the slope of decreasing of the mass fraction decreases during and after combustion, it approaches to zero at the farther distance. The porosity increase leads

to higher values of the mass fraction of gaseous fuel at the end of the first zone, but has no remarkable effect on it at the other locations. Fuel particle diameter or number density of particles increases has no effect on the temperature profile in preheating zone. In the combustion and post-flame zones, their increase is equivalent to increase of the temperature. By increasing the fuel particle diameter or increasing of the number density of particles per unit volume n_s and consequently by increasing of vaporization rate of fuel particle, the mass fraction of gaseous fuel Y has a higher value in all zones. Increase of heat loss from the system leads to the gas temperature decrease and by decreasing of temperature and vaporization rate of fuel particles, the mass fraction of gaseous fuel decreases, but is negligibly small in second and third zones. Because chemical reaction is neglected in preheating zone, there is no variation in the temperature profile with variation of combustion enthalpy, but by increasing of heat of reaction, the temperature increases in the other zones.

NOMENCLATURE

A : parameter characterizing rate of vaporization of fuel particles [kg/(m^2 K s)]
c_p : specific heat capacity [J/(kg K)]
d_p : diameter of fuel particles [m]
d_s : diameter of the solid alumina spheres [m]
d_t : diameter of tube [m]
D : molecular diffusion coefficient [m^2/s]
E : activation energy [J/mol]
h : convection heat transfer coefficient [W/(m^2 K)]
h_{eff} : effective heat transfer coefficient for heat exchange with surroundings per unit of tube diameter [W/(m^3 K)]
k_0 : Arrhenius pre-exponential factor [s^{-1}]
l : length [m]
n : temperature exponent characterizing rate of vaporization of fuel particles
n_s : local number density of particles (number of particles per unit volume) [1/m^3]
n_u : number density of particles in ambient reactant stream (number of particles per unit volume) [1/m^3]
Q : heat release per unit mass of gaseous fuel consumed [J/kg]
Q_v : heat associated with vaporizing unit mass of fuel [J/kg]
R : universal gas constant [J/(mol K)]
T_g : temperature of gas [K]
T_s : temperature of porous media [K]
t : time [s]
u_g : gas velocity [m/s]
u_{FC} : combustion wave velocity [m/s]
w_v : rate of vaporization of fuel particles [kg/(m^3 s)]
w_F : reaction rate characterizing consumption of gaseous fuel [kg/(m^3 s)]
Y : mass fraction
x : spatial distance in moving coordinates [m]
$\overline{x}$: dimensionless spatial distance
z : spatial distance [m]

Greek Letters

ε : Porosity
ε' : porous media emissivity
ε'' : transmissivity factor
λ : thermal conductivity [W/(m K)]
Λ : a small number describing the value of mass fraction of gaseous fuel at the end of the reaction zone
ρ : density [kg/m^3]
σ : Stephan-Boltzmann constant [W/(m^2 K^4)]
ν : stoichiometric coefficient

Subscripts

0 : initial condition
eff : effective
F : gaseous fuel
g : gas
O_2 : oxygen
p : fuel particles
P : product
rad : radiation
s : solid
I : first region
II : second region
III : third region

REFERENCES

1. M. R. Henneke and J. L. Ellzey, *Combust. Flame*, **117**, 832 (1999).
2. J. R. Howell, M. J. Hall and J. L. Ellzey, *Prog. Energy Combust. Sci.*, **22**, 121 (1996).
3. T. K. Kayal and M. Chakravarty, *Int. J. Heat Mass Transfer*, **48**(2), 331 (2005).
4. S. A. Zhdanok, L. A. Kennedy and G. Koester, *Combust. Flame*, **100**, 221 (1997).
5. L. A. Kennedy, J. P. Bingue, A. Saveliev, A. A. Fridman and S. I. Foutko, *Proc. Combust. Inst.*, **28**, 1431 (2000).
6. J. P. Bingue, A. V. Saveliev, A. A. Fridman and L. A. Kennedy, *Exp. Therm. Fluid Sci.*, **26**, 409 (2002).
7. J. G. Homann, R. Echigo, H. Yoshida and S. Tada, *Combust. Flame*, **111**, 32 (1997).
8. Y. Yoshizawa, K. Sasaki and R. Echigo, *Int. J. Heat Mass Transfer*, **31**, 3119 (1998).
9. S. I. Foutko, S. I. Shabunya and S. A. Zhdanok, Twenty-Sixth Symposium (Int.) on Combustion, The Combustion Institute, Naples, Italy (1996).
10. V. I. Bubnovich, S. A. Zhdanok and K. V. Dobrego, *Int. J. Heat Mass Transfer*, **49**, 2578 (2006).
11. V. Bubnovich and M. Toledo, *Appl. Therm. Eng.*, **27**(7), 1144 (2007).
12. M. A. A. Mendes, J. M. C. Pereira and J. C. F. Pereira, *Combust. Flame*, **153**, 525 (2008).
13. M. M. Kamal and A. A. Mohamad, *Proc. ImechE Part A: J. Power Energy*, **220**, 487 (2006).
14. M. Abdul Mujeebu, M. Z. Abdullah, M. Z. Abu Bakar, A. A. Mohamad, R. M. N. Muhad and M. K. Abdullah, *J. Environ. Manage.*, **90**, 2287 (2009).
15. T. K. Kayal and M. Chakravarty, *Int. J. Heat Mass Transfer*, **50**, 3359 (2007).
16. A. V. Becker, E. V. Polianczyk, N. N. Volkova and G. B. Manelis, *Theor. Found. Chem. Eng.*, **38**(5), 510 (2004).

17. J. R. Shi, M. Zh. Xie, H. Liu, G. Li and L. Zhou, *Int. J. Heat Mass Transfer*, **51**, 1818 (2008).
18. S. I. Futko, *Combust. Explosion Shock Waves*, **39**(2), 130 (2003).
19. M. Bidabadi and A. Rahbari, *Combust. Explosion Shock Waves*, **45**(3), 278 (2009).
20. F. Contarin, A. V. Saveliev, A. A. Fridman and L. A. Kennedy, *Int. J. Heat Mass Transfer*, **46**, 949 (2003).
21. E. Kreyszig, *Advanced engineering mathematics*, 9th Ed., John Wiley & Sons, Inc. (2006).
22. L. D. Smoot and P. J. Smith, *Coal combustion and gasification*, Plenum, New York (1985).